Materials for hot carrier plasmonics [Invited]

Tao Gong and Jeremy N. Munday

Department of Electrical and Computer Engineering and the Institute for Research in Electronics and Applied Physics, University of Maryland, College Park, Maryland 20742-3511, USA
**jnmunday@umd.edu*

Abstract: While the field of plasmonics has grown significantly in recent years, the relatively high losses and limited material choices have remained a challenge for the development of many device concepts. The decay of plasmons into hot carrier excitations is one of the main loss mechanisms; however, this process offers an opportunity for the direct utilization of loss if excited carriers can be collected prior to thermalization. From a materials point-of-view, noble metals (especially gold and silver) are almost exclusively employed in these hot carrier plasmonic devices; nevertheless, many other materials may offer advantages for collecting these hot carriers. In this manuscript, we present results for 16 materials ranging from pure metals and alloys to nanowires and graphene and show their potential applicability for hot carrier excitation and extraction. By considering the expected hot carrier distributions based on the electron density of states for the materials, we predict the preferred hot carrier type for collection and their expected performance under different illumination conditions. By considering materials not traditionally used in plasmonics, we find many promising alternative materials for the emerging field of hot carrier plasmonics.

OCIS codes: (250.5403) Plasmonics; (160.0160) Materials; (040.5160) Photodetectors.

References and links

1. C. Clavero, "Plasmon-induced hot-electron generation at nanoparticle/metal-oxide interfaces for photovoltaic and photocatalytic devices," Nat. Photonics **8**(2), 95–103 (2014).
2. M. L. Brongersma, N. J. Halas, and P. Nordlander, "Plasmon-induced hot carrier science and technology," Nat. Nanotechnol. **10**(1), 25–34 (2015).
3. M. W. Knight, H. Sobhani, P. Nordlander, and N. J. Halas, "Photodetection with active optical antennas," Science **332**(6030), 702–704 (2011).
4. A. Sobhani, M. W. Knight, Y. Wang, B. Zheng, N. S. King, L. V. Brown, Z. Fang, P. Nordlander, and N. J. Halas, "Narrowband photodetection in the near-infrared with a plasmon-induced hot electron device," Nat. Commun. **4**, 1643 (2013).
5. M. W. Knight, Y. Wang, A. S. Urban, A. Sobhani, B. Y. Zheng, P. Nordlander, and N. J. Halas, "Embedding plasmonic nanostructure diodes enhances hot electron emission," Nano Lett. **13**(4), 1687–1692 (2013).
6. F. P. G. de Arquer, A. Mihi, and G. Konstantatos, "Large-area plasmonic-crystal-hot-electron-based photodetectors," ACS Photonics **2**(7), 950–957 (2015).
7. P. Reineck, G. P. Lee, D. Brick, M. Karg, P. Mulvaney, and U. Bach, "A solid-state plasmonic solar cell via metal nanoparticle self-assembly," Adv. Mater. **24**(35), 4750–4755, 4729 (2012).
8. W. Li and J. Valentine, "Metamaterial perfect absorber based hot electron photodetection," Nano Lett. **14**(6), 3510–3514 (2014).
9. F. Wang and N. A. Melosh, "Plasmonic energy collection through hot carrier extraction," Nano Lett. **11**(12), 5426–5430 (2011).
10. H. Chalabi, D. Schoen, and M. L. Brongersma, "Hot-electron photodetection with a plasmonic nanostripe antenna," Nano Lett. **14**(3), 1374–1380 (2014).
11. T. Gong and J. N. Munday, "Angle-independent hot carrier generation and collection using transparent conducting oxides," Nano Lett. **15**(1), 147–152 (2015).
12. H. A. Atwater, "The promise of plasmonics," Sci. Am. **296**(4), 56–62 (2007).
13. M. J. Mendes, A. Luque, I. Tobias, and A. Marti, "Plasmonic light enhancement in the near-field of metallic nanospheroids for application in intermediate band solar cells," Appl. Phys. Lett. **95**(7), 071105 (2009).

#249149 Received 31 Aug 2015; revised 4 Oct 2015; accepted 4 Oct 2015; published 12 Oct 2015

Corrected: 24 November 2015

14. T. P. White and K. R. Catchpole, "Plasmon-enhanced internal photoemission for photovoltaics: theoretical efficiency limits," Appl. Phys. Lett. **101**(7), 073905 (2012).
15. R. Sundararaman, P. Narang, A. S. Jermyn, W. A. Goddard 3rd, and H. A. Atwater, "Theoretical predictions for hot-carrier generation from surface plasmon decay," Nat. Commun. **5**, 5788 (2014).
16. M. K. Hedayati, F. Faupel, and M. Elbahri, "Review of plasmonic nanocomposite metamaterial absorber," Materials (Basel) **7**(2), 1221–1248 (2014).
17. J. A. Bossard, L. Lin, S. Yun, L. Liu, D. H. Werner, and T. S. Mayer, "Near-ideal optical metamaterial absorbers with super-octave bandwidth," ACS Nano **8**(2), 1517–1524 (2014).
18. J. Spitaler and L. Pardini, "Electronic-Structure Calculations," http://exciting-code.org/beryllium-electronic-structure-calculations.
19. L. H. Bennett, *Electronic Density of States: Based on Invited and Contributed Papers and Discussion* (U.S. National Bureau of Standards, 1971).
20. F. Pauly, J. K. Viljas, U. Huniar, M. Hafner, S. Wohlthat, M. Burkle, J. C. Cuevas, and G. Schon, "Cluster-based density-functional approach to quantum transport through molecular and atomic contacts," New J. Phys. **10**(12), 125019 (2008).
21. D. R. Mason, C. P. Race, M. H. F. Foo, A. P. Horsfield, W. M. C. Foulkes, and A. P. Sutton, "Resonant charging and stopping power of slow channelling atoms in a crystalline metal," New J. Phys. **14**(7), 073009 (2012).
22. K. Krupski, M. Moors, P. Jozwik, T. Kobiela, and A. Krupski, "Structure determination of Au on Pt(111) surface: LEED, STM and DFT Study," Materials (Basel) **8**(6), 2935–2952 (2015).
23. M. Jafari, H. Jamnezhad, and L. Nazarzadeh, "Electronic properties of titanium using density functional theory," Iranian J. Sci. and Tech. **36**, 511–515 (2012).
24. S. Kanagaprabha, A. T. Asvinimeenaatci, G. Sudhapriyanga, A. Jemmy Cinthia, R. Rajeswarapalanichamy, and K. Iyakutti, "First principles study of stability and electronic structure of TMH and TMH_2 (TM = Y, Zr, Nb)," Acta Phys. Pol. A **123**, 126–131 (2013).
25. M. A. Ortigoza and T. S. Rahman, "First principles calculations of the electronic and geometric structure of $Ag_{27}Cu_7$ Nanoalloy," Phys. Rev. B **77**(19), 195404 (2008).
26. A. Kumar and D. P. Ojha, "Electrical transport and electronic structure calculation of Al-Ga binary alloys," Acta Phys. Pol. A **119**, 408–415 (2011).
27. V. Fournee, I. Mazin, D. A. Papaconstantopoulos, and E. Belin-Ferre, "Electronic structure calculations of Al-Cu alloys: comparison with experimental results on Hume-Rothery phases," Philos. Mag. B **79**(2), 205–221 (1999).
28. A. Kumar, D. Banyai, P. K. Ahluwalia, R. Pandey, and S. P. Karna, "Electronic stability and electron transport properties of atomic wires anchored on the MoS_2 monolayer," Phys. Chem. Chem. Phys. **16**(37), 20157–20163 (2014).
29. E. Faizabadi, "Single wall carbon nanotubes in the presence of vacancies and related energy gaps," in *Electronic Properties of Carbon Nanotubes*, J. M. Marulanda, ed. (Intech, 2011).
30. K. Nakada and A. Ishii, "DFT Calculation for Adatom Adsorption on Graphene," in *Graphene Simulation*, J. R. Gong, ed. (Intech, 2011).
31. E. Y. Chan, H. C. Card, and M. C. Teich, "Internal photoemission mechanisms at interfaces between germanium and thin metal films," IEEE J. Quantum Electron. **16**(3), 373–381 (1980).
32. A. J. Leenheer, P. Narang, N. S. Lewis, and H. A. Atwater, "Solar energy conversion via hot electron internal photoemission in metallic nanostructures: efficiency estimates," J. Appl. Phys. **115**(13), 134301 (2014).
33. A. Manjavacas, J. G. Liu, V. Kulkarni, and P. Nordlander, "Plasmon-induced hot carriers in metallic nanoparticles," ACS Nano **8**(8), 7630–7638 (2014).
34. A. O. Govorov and H. Zhang, "Kinetic density functional theory for plasmonic nanostructures: breaking of the plasmon peak in the quantum regime and generation of hot electrons," J. Phys. Chem. C **119**(11), 6181–6194 (2015).
35. K. J. Tielrooij, M. Massicotte, L. Piatkowski, A. Woessner, Q. Ma, P. Jarillo-Herrero, N. F. van Hulst, and F. H. L. Koppens, "Hot-carrier photocurrent effects at graphene-metal interfaces," J. Phys.- Condensed Mat. **27**, 16 (2015).
36. K. J. Tielrooij, J. C. W. Song, S. A. Jensen, A. Centeno, A. Pesquera, A. Z. Elorza, M. Bonn, L. S. Levitov, and F. H. L. Koppens, "Photoexcitation cascade and multiple hot-carrier generation in graphene," Nat. Phys. **9**(4), 248–252 (2013).
37. D. Sun, G. Aivazian, A. M. Jones, J. S. Ross, W. Yao, D. Cobden, and X. Xu, "Ultrafast hot-carrier-dominated photocurrent in graphene," Nat. Nanotechnol. **7**(2), 114–118 (2012).

1. Introduction

Hot carrier effects in metals have drawn significant attention recently because of their promising applications in photodetection, energy-harvesting, hot-carrier-induced chemistry, etc. [1–4]. Hot carrier collection enables utilization of energy that is usually lost in a conventional semiconductor device due to thermalization (*i.e.* phonon generation and heat dissipation resulting from absorption of high energy photons) and sub-bandgap photon loss (*i.e.* lack of absorption of low energy photons). This energy can be extracted through the hot carrier generation in a metal and the subsequent injection of the carrier into a semiconductor

#249149 Received 31 Aug 2015; revised 4 Oct 2015; accepted 4 Oct 2015; published 12 Oct 2015

(M-S) [4–8] or a counter-electrode (M-I-M) [9–11]. In order to achieve high efficiency hot carrier injection, significant light absorption is required in the metal, which is achievable by coupling incident light into surface plasmons (SP)—the collective oscillation of free electrons near the metal surface [2, 12, 13]. The improved absorption contributes greatly to the enhancement of hot carrier generation and consequently increases the device efficiency. Therefore, surface plasmons effects are often employed for hot carrier generation.

While most hot carrier devices to-date have used Au or Ag nanostructures, due to their chemical stability and well-studied plasmonic properties, other materials might have potential advantages from the perspective of hot carrier generation following absorption. The hot carrier injection efficiency depends not only on the light absorption, which is made possible by surface plasmon excitation, but also on the hot carrier energy distribution upon excitation, resulting from the decay of the surface plasmons [14, 15]. The hot carrier energy distribution is critical for the collection of carriers because only the hot carriers with sufficiently high energy and momentum are able to traverse the barrier established at the interface between the metal and the semiconductor or oxide. The hot carrier energy distribution immediately after photon absorption is determined by the initial states of electrons in the Fermi gas and the incident photon energy. Here we present the hot carrier energy distributions in various materials (including metals, alloys, and nanostructures) based on the electron density of states (EDOS) determined by first principle calculations or experiments from the literature. We compare these distributions to the idealized distributions that would optimize the hot carrier injection. These results are meant to outline materials and nanostructures that might be more suitable for hot carrier collection and to provide an alternative perspective on choosing plasmonic materials when the goal is hot carrier generation.

In this manuscript we present the hot carrier distributions for electrons and holes in a variety of pure metals (Au, Ag, Cu, Al, Fe, Pt, Ti, and Y), alloys (Ag-Cu, Al-Ga, Au-Pt, and Al-Cu), and nanostructures (Ag and Au nanowires, carbon nanotubes, and graphene). In order to determine the expected hot carrier distributions, we first assume complete absorption within the material through perfect coupling of the incident light into surface plasmons. This assumption serves to eliminate the influence of the optical absorption on the resulting carrier distribution and allows us to focus solely on the influence of the EDOS. Further, nearly perfect absorption has been experimentally achieved in a number of plasmonic and metamaterial structures [4, 8, 16, 17]. Secondly, EDOS data are taken from the literature [18–30]. Combining the EDOS with the Fermi distribution function yields the transition probability and hence the resulting hot carrier distribution. Alternatively, the transition probability under illumination can be calculated from first principles using Fermi's golden rule for the transition, governed by quantum mechanical selection rules. However, the EDOS method turns out to have worked well to describe the performance of previous hot carrier devices [9, 10] and will be used here to evaluate the potential of different materials for hot carrier devices.

2. Simple models for the hot carrier distribution

The simple model of a metal consists of free electrons moving through a metallic ion lattice, resulting in the well-known parabolic electron density of states (Fig. 1(a)), $D(E) \propto \sqrt{E}$, where $D(E)$ is the electron density of states as a function of the electron energy. Upon photon excitation with energy E_{ph}, an electron in the Fermi gas is promoted from E-E_{ph} to a higher energy state E. The transition probability is proportional to the multiplication of the joint density of states, which is the product of the densities of states at the initial and final energies, and their respective distribution functions:

$$P(E) \propto D(E - E_{ph}) f(E - E_{ph}) D(E)(1 - f(E))$$

#249149 Received 31 Aug 2015; revised 4 Oct 2015; accepted 4 Oct 2015; published 12 Oct 2015

where $f(E)$ is the Fermi distribution function.

Upon monochromatic illumination (λ = 600 nm), a nearly uniform hot carrier distribution is generated based on the parabolic EDOS (Fig. 1(b)). This uniform distribution is not ideal for hot carrier collection, because many of the carriers will not have enough energy to overcome the interface barrier, Φ_B. Hence a large fraction of hot carriers with low energy would be lost.

Under broadband AM1.5G solar illumination, both the hot electron and hole distributions are concentrated close to the Fermi energy, E_F (Fig. 1(c)). The resulting distribution is obtained because all incident photons (regardless of energy) can yield hot carrier distributions near the Fermi energy; however, only high energy photons result in hot carrier distributions far from the Fermi energy. Thus, this distribution profile is even less favorable for hot carrier injection than the distribution yielded by monochromatic light, because a smaller fraction of the carriers have the required high energy needed for injection.

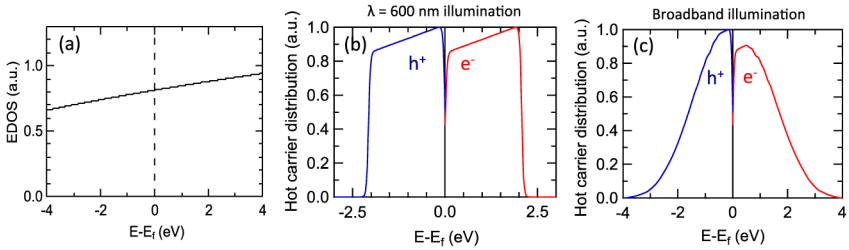

Fig. 1. Calculations of hot carrier distributions based on the ideal free electron model. (a) Parabolic EDOS as a function of energy (electron energy minus Fermi energy) where E_F is ~11.7 eV for a metal like Al. EDOS is relatively flat for carriers with energies within ± 4 eV of the Fermi energy. (b) Hot carrier energy distribution upon excitation by 600 nm illumination (2.07 eV). Nearly uniform distributions for both hot electrons and holes are obtained. (c) Hot carrier energy distribution under broadband illumination (*i.e.* AM1.5G solar spectrum). The distribution is centralized near the Fermi level for both carriers, which is less favorable for hot carrier injection.

While the parabolic EDOS model is often used to describe an ideal metal, real materials usually do not exhibit the ideal parabolic EDOS behavior owing to band overlapping, various crystallographic orientations, nanoscale confinement, etc. Instead, a more complicated EDOS is commonly observed, which may contain peaks in the hot carrier distributions. Because different materials depart from the parabolic EDOS in different ways, it is important to understand how these changes effect the resulting hot carrier distributions.

To improve the hot carrier distributions, we consider a shifted parabolic EDOS model, where a parabolic EDOS is still used; however, the band edge is assumed to be just below the Fermi level (~0.15 eV below, see Fig. 2(a)). This model was first presented to describe experimental photoemission results obtained from thin metallic films on Ge [31] and results in an excited electron energy distribution with a single peak for hot carriers, arising from the excitation of electrons close to the Fermi energy. This model results in a high concentration of Fermi gas electrons within an extremely narrow energy range close to the Fermi level at thermal equilibrium. Thus, the excited hot electrons are also distributed within a narrow energy range (Fig. 2(b)). The peaked distribution is beneficial for hot electron injection, provided the barrier height Φ_B is appropriately chosen for the input illumination spectrum. For example, for Φ_B < 3 eV, the hot electrons excited by 400 nm photons will be able to get over the barrier and create photocurrent, as they possess energy greater than 3 eV (Fig. 2(b)).

Under broadband AM1.5G illumination, the modified EDOS model also yields a better distribution than the parabolic EDOS. As shown in Fig. 2(d), the distribution is more highly weighted towards higher energies rather than centralized near the Fermi level. Moreover, this distribution can be further improved by additional modifications to the EDOS profile.

#249149 Received 31 Aug 2015; revised 4 Oct 2015; accepted 4 Oct 2015; published 12 Oct 2015

Specifically, it is desirable to have an EDOS increase more steeply as a function of energy. As mentioned in the above analysis, the large concentration of Fermi gas electrons very close to the Fermi level is modeled by an effective conduction band edge just below the Fermi energy; however, the resulting hot electron energy distribution also relies on the density of the unoccupied energy states one photon energy above the Fermi level. Therefore, if the density of the unoccupied states is larger, the final distribution would be pushed further into the higher energy range under broadband illumination. Thus, we consider two additional EDOS models that increase more steeply with energy than the parabolic model ($\sqrt{E}$): E^2 and $\exp(E)$. Figure 2(c) shows these two other EDOS models, both of which yield a narrowband equilibrium electron distribution just below the Fermi level; however, above the Fermi level, the density of vacant states increase faster with energy than $\sqrt{E}$ (*i.e.* as E^2 or $\exp(E)$). Though the peaked distributions under monochromatic light illumination for the three models are expected to be similar, the much larger number of vacant states in the latter two models further increases the probability of transitions into higher energy states, pushing the energy distribution of hot electrons further into the higher energy range when under broadband solar illumination (Fig. 2(d)). While the above EDOS models have been described for the hot electron distributions, similar expressions hold for hot hole distributions; however, for the ideal hole case, a narrowband of occupied electron states exist below the Fermi level and few vacant states exist above it.

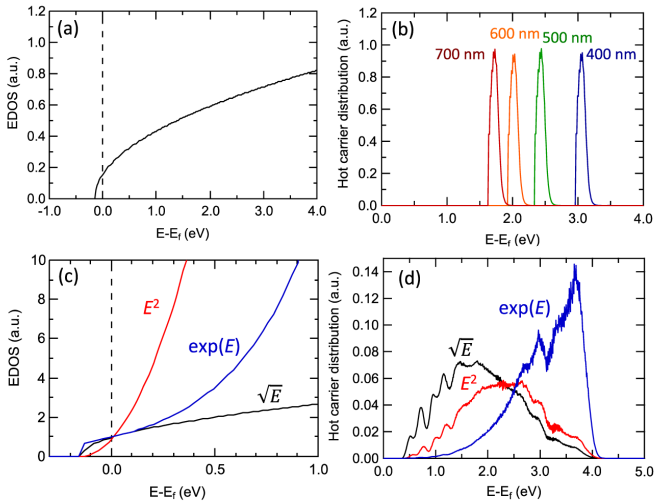

Fig. 2. Calculation of hot carrier distributions based on the modified EDOS models. (a) Ideal parabolic EDOS with the Fermi level extremely close to the band edge, leaving a large concentration of Fermi gas electrons within a narrow energy range below the Fermi energy. (b) Hot electron energy distribution under illumination by monochromatic light using the EDOS of (a). The hot carrier distribution has a peak that shifts toward higher energy as the energy of the absorbed photon increases. (c) Alternative EDOS distributions yielding higher densities of vacancy states above the Fermi level. Three models (EDOS varies as ~ $\sqrt{E}$, ~E^2, or ~exp(E)) are considered for the modified EDOS. (d) The resulting hot electron distributions under AM1.5G illumination shift toward higher energies for EDOS functions that increase more rapidly with E. Distributions with a larger fraction of high energy carriers are more favorable for hot electron extraction under broad-band illumination.

3. Hot carrier distributions in real metals

The hot carrier distributions for real metals may vary significantly from the simple models presented in section 2. Metals are the most commonly used materials for exciting surface

#249149 Received 31 Aug 2015; revised 4 Oct 2015; accepted 4 Oct 2015; published 12 Oct 2015

plasmons to generate hot carriers due to their high free carrier densities, and Ag [18], Al [19], Au [20] and Cu [21] are among the most extensively studied metals for plasmonics. However, with the exception of Al, the EDOS profiles for these metals do not resemble either the ideal parabolic EDOS or any of the modified EDOS. Instead, large numbers of occupied states are found below the Fermi level (Fig. 3). The departure of the EDOS from the simple models suggests that the hot carrier distributions generated from photo-excitation may also vary significantly from the idealized models.

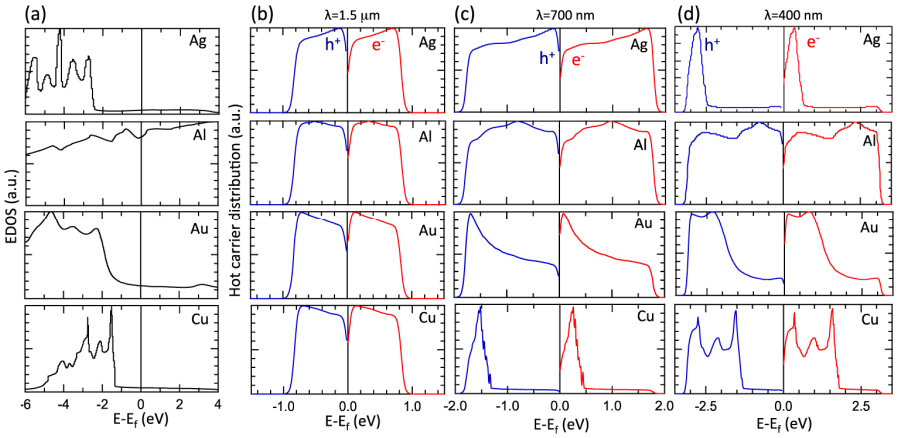

Fig. 3. EDOS and hot carrier distributions for common plasmonic materials: Ag, Al, Au and Cu. (a) EDOS for these four materials. Except Al, all of these materials exhibit a much higher density of states below the Fermi level. Under monochromatic illumination, hot carrier distributions are created from incident photons with wavelengths: (b) 1.5 μm (0.83 eV), (c) 700 nm (1.78 eV), and (d) 400 nm (3.11 eV). Low photon energies yield relatively uniform hot carrier distributions for all four metals; however, upon higher energy illumination, peaks begin to appear due to high densities of occupied states below the Fermi level for Ag, Au, and Cu. Under 700 nm illumination Au and Cu are more efficient in hole extraction than electron extraction because the distribution of hot holes is peaked further from the Fermi level.

The generated hot carrier distribution depends not only on the EDOS, but also on the energy of the incident photons. Usually in a silicon-based M-S hot carrier device, the sub-bandgap photons are in the near-IR range with relatively low energy. As shown in Fig. 3(b), the 0.83 eV (1.5 μm) photons generate both hot electron and hole distributions almost uniformly above and below the Fermi energy. This nearly uniform response is because close to the Fermi level (*i.e.* within one photon energy), the EDOS is relatively flat in these metals. However, a higher photon energy of 1.78 eV (700 nm) yields a different distribution for Au and Cu because the relatively large density of states far below the Fermi energy comes into play, contributing significantly to the electron transition process. For these metals, the large concentration of Fermi gas electrons about one photon energy below the Fermi level is a result of band overlapping (d-band) [15, 32]. Therefore, a distinct peak occurs in the hot electron distribution just above the Fermi level (Fig. 3(c)). Similarly, a peak in the hot carrier distribution also appears in Ag (Fig. 3(d)) if the photon energy is much higher (>3 eV), but the 1.78 eV photons do not have enough energy to excite this transition (Fig. 3(c)). Al, on the contrary, has an EDOS that is closest to an ideal parabola, resulting in a uniform hot carrier distribution for all wavelengths considered.

Because the EDOS is not symmetric about the Fermi energy for many materials, different materials will perform better for electron or hole extraction. For Au and Cu, the peaks in the hot carrier distributions are much further from the Fermi level for hot holes than for hot electrons. Thus, hot hole extraction is much more favorable because they are more likely to have enough energy to traverse the energy barrier and be collected in the counter-electrode. This observation agrees with the results derived from first principles calculations [15].

#249149 Received 31 Aug 2015; revised 4 Oct 2015; accepted 4 Oct 2015; published 12 Oct 2015

Although the above metals are most widely used in plasmonics, they might not be the best for the purpose of hot carrier generation. Here we explore several other metals and demonstrate their potential for hot carrier effects (Fig. 4). Included are transition metals and rare-earth metals, which involve more complicated EDOS profiles due to their complex band structures. For Pt [22], due to the large number of occupied states below the Fermi level, the peak for hot holes is still much further from the Fermi level than that for hot electrons, making it better suited for hot hole collection than hot electron collection. For the other metals listed here, a high EDOS appears on both sides of the Fermi level. Ti [23] works fairly well for both carrier types. Y [24] appears better for hot electron collection under 700 nm illumination but generates similar distributions for hot electrons and holes under 400 nm illumination. A different effect occurs in Fe [19], where hot electrons are more easily collected under 400 nm illumination, but 700 nm illumination favors the hot hole collection. In general, one needs to consider both the EDOS profile and the photon excitation energy to determine which carrier type is most efficiently injected/collected.

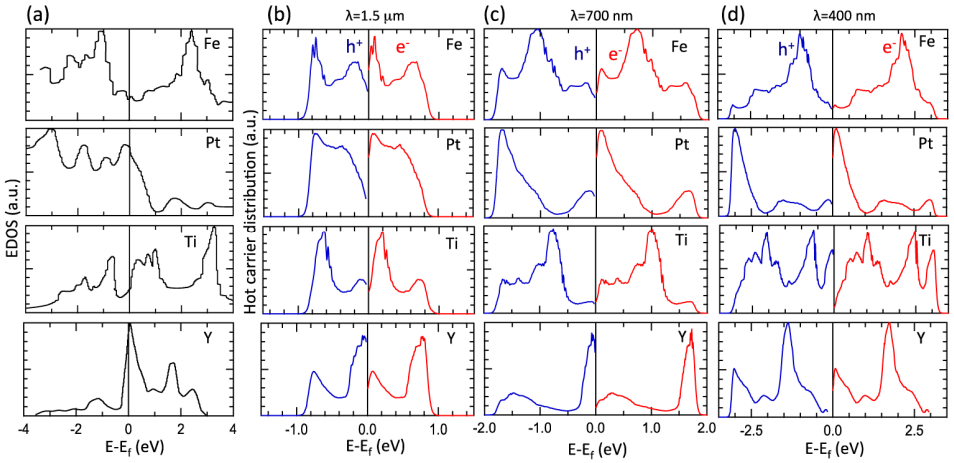

Fig. 4. EDOS and hot carrier distributions for Fe, Pt, Ti and Y. (a) More complex EDOS profiles are obtained for these metals as a result of their more complicated band structures. Hot carrier distributions are excited by (b) 1.5 μm (0.83 eV), (c) 700 nm (1.78 eV), and (d) 400 nm (3.11 eV) illumination. More complex patterns in the hot carrier distributions are observed, and the relative positions of peaks (and hence the preferred carrier collection types) depend on the incident photon energy.

4. Hot carrier distributions in alloys

Unlike pure metals, alloys enable the engineering the EDOS through the control over synthesis conditions. The compositions and crystallographic orientations can be varied, enabling more complexity and tunability than pure metals. Figure 5 shows the EDOS of an Ag-Cu alloy ($Ag_{27}Cu_7$) [25], which is very different than the EDOS of either Ag or Cu individually (Fig. 3). Thus, the hot carrier distributions of the alloy are also significantly different than either of the pure metals. When excited by 700 nm wavelength light, the Ag-Cu alloy better supports hot electron collection because the hot electron distribution's peak is further away from the Fermi level. This behavior is in contrast to the uniform hot carrier distribution of Ag or the preferred hot hole collection in Cu at this illumination wavelength. For the Al-Ga alloy (equiatomic composition) [26], the distributions are relatively flat but slightly favor hot hole collection. For Au-Pt alloy (Au atoms sitting in the most stable hollow FCC positions on the Pt (111) lattice) [22], the EDOS is close to the ideally modified profile for holes, where there is high density for occupied states below the Fermi level, but low density for vacant states above the Fermi level. This profile would best facilitate hot hole

#249149 Received 31 Aug 2015; revised 4 Oct 2015; accepted 4 Oct 2015; published 12 Oct 2015

extraction regardless of the photon energy because the hot hole distribution peak will always be as far as possible from the Fermi energy.

The biggest advantage of using alloys is that it provides tunability of hot carrier generation, so one can engineer the EDOS of an alloy according to one's needs. For instance, in Al-Cu alloy ($AlCu_3$) [27], the occupied states with large density are pushed further away from the Fermi level in the EDOS profile compared with the Cu EDOS. Though this distribution is not beneficial for broadband illumination, it favors the hot hole extraction for higher energy photons than Cu, which might prove useful for short wavelength photodetection if the barrier height is appropriately chosen.

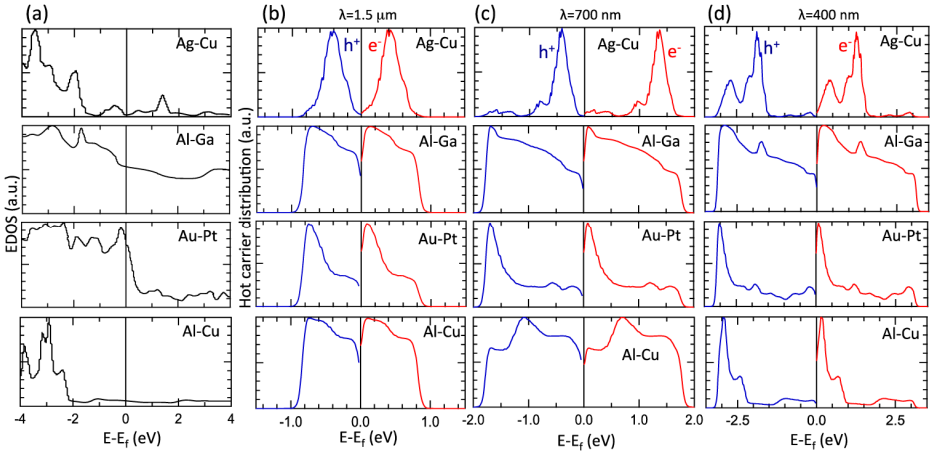

Fig. 5. EDOS and hot carrier distributions for various alloys. (a) The EDOS of alloys can be engineered so that they differ significantly from their component metals. Hot carrier energy distribution upon excitation by (b) 1.5 μm, (c) 700 nm, and (d) 400 nm illumination. As in pure metals, the peaks in the distribution vary with both material choice and photon excitation energy. By varying the alloy composition, a range of EDOS possibilities is expected for each of the alloys.

5. Hot carrier distributions in nanostructures

Nanostructure confinement is an alternative approach to modifying the EDOS of a metal. As the dimensions of the structure are reduced to the nanometer scale or even smaller, the electron wavefunctions change dramatically, consequently changing the EDOS [33]. A recent theoretical work using the kinetic DFT method has also systematically studied the influence of the metal nanocrystal confinement on the plasmonic absorption and hot carrier generation [34]. This effect provides another possibility for tuning hot carrier generation. Figure 6 shows the EDOS of Ag and Au nanowires (monoatomic wires anchored on a MoS_2 monolayer) [28], which is dramatically different from their bulk counterparts. 700 nm illumination, which yields a uniform hot carrier distribution in Ag, gives rise to distinctive peaks in the distribution of both carrier types for the Ag nanowire, as a result of a new peak induced close to the Fermi level in its EDOS profile. For the Au nanowire, a more complex EDOS is found below the Fermi level resulting in multiple peaks in the hot carrier distribution, for both electrons and holes. Compared to bulk Au, more occupied states exist just below the Fermi level in the nanowire structure, which enables lower energy photons to excite the carriers into the peak distribution. Generally, the nanoscale confined metals behave completely differently than bulk metals in terms of hot carrier generation, and specific designs should be considered independently.

#249149 Received 31 Aug 2015; revised 4 Oct 2015; accepted 4 Oct 2015; published 12 Oct 2015

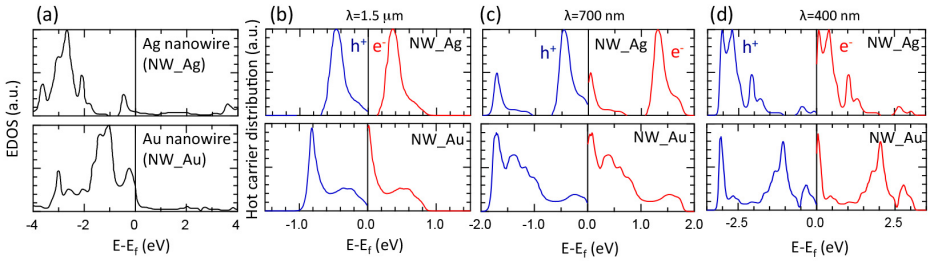

Fig. 6. EDOS and hot carrier distributions for monoatomic nanowires of Ag and Au. (a) Nanowire EDOS show more complicated behavior than their bulk counterparts. Similarly, the generated hot carrier distributions upon excitation by (b) 1.5 μm, (c) 700 nm, and (d) 400 nm illumination show multiple peaks instead of a more uniform distribution or a single peak, as is found in the bulk. Generally, nanoscale confined metals have different hot carrier distributions, and specific designs should be considered for different applications.

In addition to nanostructured metals, some non-metallic nanostructures could also be a promising option for hot carrier generation. Carbon-nanotubes (CNTs) and graphene have been extensively studied for various applications, and interest has recently emerged in hot carrier effects [35–37]. Through the modification of geometry, dimensions, and doping, CNTs and graphene are able to transform their EDOS profile to a great extent, showing promise for applications in hot carrier generation.

As shown in Fig. 7(a), the CNTs (zig-zag single-wall CNT (11, 0) with a single vacancy) [29] have an EDOS that exhibits a narrowly peaked density of states around the Fermi energy, resulting in one peak in the hot carrier distribution at an energy of 2.49 eV (under 500 nm illumination, Fig. 7(d)) and another very close to the Fermi level. Because the central peak concentrates nearly half of the total excited carriers in a very small energy range, this distribution is not as favorable for hot carrier extraction; however, it is still more advantages than a uniform distribution from the perspective of the flexibility of barrier height choice. In this particular case, as long as $\Phi_B < 2.49$ eV, the hot carriers in the main peak would all be collected, independent of the barrier height; whereas with a uniform distribution, the barrier height would significantly influence the extraction efficiency. Graphene [30], on the contrary, has almost no states at the Fermi level, but has narrow peaks in the EDOS on both sides of the Fermi level when illuminated at 500 nm. Consequently, a distinct narrow peak distribution is yielded for both hot electrons and holes, which facilitates the extraction of both carriers.

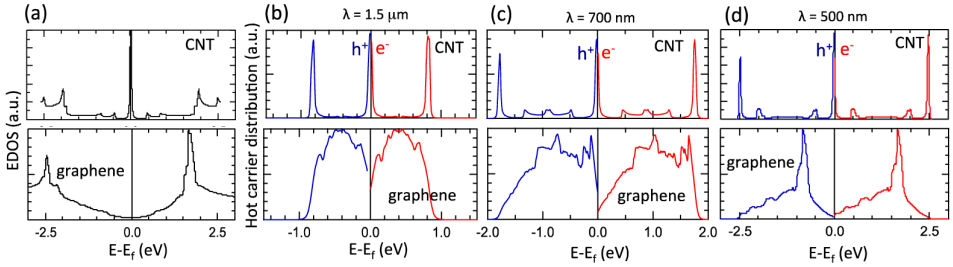

Fig. 7. EDOS and hot carrier distributions for CNT and graphene. (a) EDOS are nearly symmetric for both materials and have distinctive narrow peaks. Hot carrier energy distribution upon excitation by (b) 1.5 μm, (c) 700 nm, and (d) 500 nm illumination show narrow peaks, which are favorable for hot carrier injection. We note that the EDOS of CNT and graphene are extremely sensitive to changes in geometry, dimensions, doping, etc., which add additional flexibility to tuning the EDOS profile.

#249149 Received 31 Aug 2015; revised 4 Oct 2015; accepted 4 Oct 2015; published 12 Oct 2015

6. Hot carrier distributions under broadband illumination

We have shown hot carrier distributions in various materials and nanostructures under monochromatic illumination. These results are summarized in Table 1 for illumination wavelengths of 400 nm, 700 nm, and 1500 nm. If both carrier types show a relatively flat distribution, both carrier types are considered suitable for collection. If there are peaks in the distribution, we compare the separation between the main peak and the Fermi level to determine which carrier type is better suited for extraction. Of course, the actual collection efficiencies will also depend upon the interface barrier height, which depends on the details of the device under consideration. This table is meant to provide rough guidance for the choice of the preferred carrier type for extraction.

Table 1. Summary of expected hot carrier collection efficiencies for electrons and holes under illumination (400 nm, 700 nm, or 1.5 μm) for the materials considered in this manuscript. Checkmarks suggest, as a rough guide, that a particular carrier type is preferred for collection. If both electrons and holes have a checkmark, both carrier types are expected to be collected. The actual collection efficiencies will also depend upon the interface barrier height, which depends on the details of the device under consideration.

Illumination wavelength:	**400 nm**		**700 nm**		**1500 nm**	
Carriers efficiently collected:	**Hot electrons**	**Hot holes**	**Hot electrons**	**Hot holes**	**Hot electrons**	**Hot holes**
Pure metals						
Ag		✓	✓	✓	✓	✓
Al	✓	✓	✓	✓	✓	✓
Au		✓		✓	✓	✓
Cu		✓		✓	✓	✓
Fe	✓		✓	✓	✓	✓
Pt		✓		✓	✓	✓
Ti	✓	✓	✓	✓		✓
Y	✓	✓	✓		✓	
Alloys						
Ag-Cu		✓	✓		✓	✓
Al-Ga	✓	✓	✓	✓	✓	✓
Au-Pt		✓		✓		✓
Al-Cu		✓	✓	✓	✓	✓
Nanostructures						
Ag nanowire		✓	✓		✓	✓
Au nanowire	✓	✓		✓		✓
CNT	✓	✓	✓	✓	✓	✓
Graphene	✓	✓	✓	✓	✓	✓

#249149 Received 31 Aug 2015; revised 4 Oct 2015; accepted 4 Oct 2015; published 12 Oct 2015

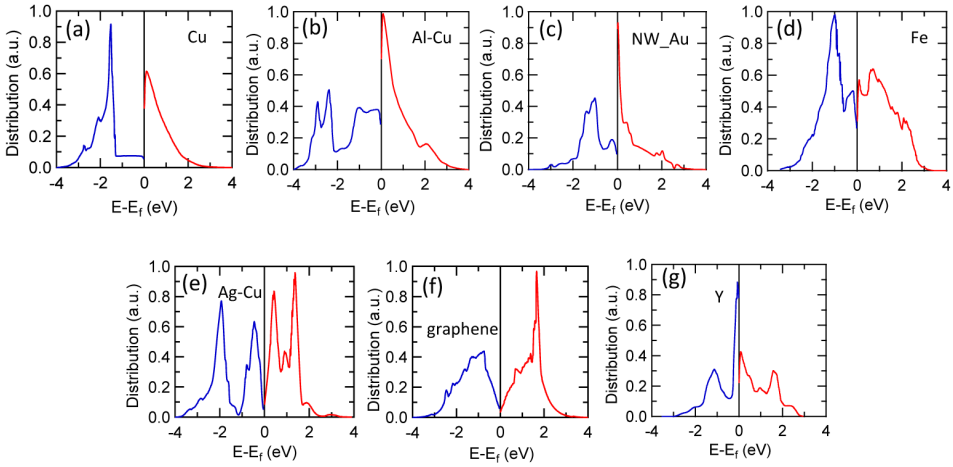

Fig. 8. Hot carrier distributions for different materials under AM1.5G illumination. In (a), (b) and (c), hot holes distributions are weighted further from the Fermi level, indicating suitability for hot hole extraction. In (d) and (e), comparable distributions for both carriers are found. In (f) and (g), hot electrons are slightly preferred due to an overall larger fraction of excited electrons further from the Fermi level.

Under broadband illumination, the hot carrier distributions are similarly varied depending on the material choice. As indicated in Fig. 1(c), the ideal parabolic EDOS model does not yield a preferable distribution because both carriers will be predominantly concentrated near the Fermi level. The modified EDOS models (Fig. 2(d)) extend the generated hot electron distributions to a higher energy range due to the concentrated electrons in the Fermi gas close to the Fermi level and large density of vacant states above the Fermi level (or vice versa for hot hole generation). For real materials, the EDOS is much more complicated. Figure 8 demonstrates the hot carrier distributions in several of the materials presented in this manuscript under broadband solar illumination. For Cu, Al-Cu alloy and Au nanowires (Figs. 8(a)-8(c)), hot electrons are still predominantly generated close to the Fermi level, as in the ideal parabolic EDOS case. However, hot holes are shifted further from the Fermi level, which results from the much larger EDOS below the Fermi level than above the Fermi level. The hot hole collection is hence more favorable in these materials. For Fe and Ag-Cu alloys (Figs. 8(d) and 8(e)), both carriers spread into the higher energy range due to the relatively symmetric and large EDOS profile about the Fermi level. These materials can thus be utilized equally well for collection of both carrier types. For graphene and Y (Figs. 8(f) and 8(g)), hot electrons are distributed further from the Fermi level, owing to the larger EDOS above the Fermi level in the two materials, which renders slightly more efficient hot electron extraction.

7. Conclusions

In conclusion, we have described a variety of alternative materials that can be used in hot carrier plasmonics. We have calculated the excited hot carrier energy distributions for a variety of materials and nanostructures based on their EDOS and have compared these results with simplified cases that are commonly used in the literature. We have shown preferred hot carrier extraction for electrons or holes depends on the chosen material and illumination wavelength. As expected, these materials have demonstrated great variability in their hot carrier generation profiles, showing the usefulness of different materials for specific applications. The design principles for hot carrier plasmonics are indeed different from those in traditional plasmonics and alternative material choices will be important as the field progresses.

#249149 Received 31 Aug 2015; revised 4 Oct 2015; accepted 4 Oct 2015; published 12 Oct 2015

Acknowledgments

We acknowledge partial support by the University of Maryland through start-up funds and a Research and Scholarship Award (RASA).

#249149 Received 31 Aug 2015; revised 4 Oct 2015; accepted 4 Oct 2015; published 12 Oct 2015